ELSEVIER

Journal of Chromatography A, 722 (1996) 3–17

JOURNAL OF CHROMATOGRAPHY A

Three-dimensional molecular simulation of chromatographic separations

Victoria L. McGuffin*, Peiru Wu

Department of Chemistry, Michigan State University, East Lansing, MI 48824-1322, USA

Abstract

A three-dimensional stochastic computer simulation has been developed in order to provide a detailed understanding of chromatographic separations. In this simulation, the migration of individual molecules is established through diffusion and convection within a fluid phase that is in contact with a surface. Molecular interaction and, hence, retention may arise by partitioning into permeable surfaces or by adsorption at solid surfaces. The molecular distribution and the corresponding zone profile may be examined and characterized by means of statistical moments at any specified time or spatial position during the simulation. This simulation provides a powerful and versatile model with which to characterize transport phenomena in complex chromatographic separation systems.

1. Introduction

Much of our current understanding of chromatography has been obtained through the correlation of experimental measurements with theoretical models. The development of more powerful and comprehensive models is necessary to define and clarify the current status as well as to guide future advances in separation science.

A variety of classical models has been used to describe transport phenomena in chromatographic systems [1–5]. These classical models, which are developed from macroscopic principles and properties, yield the cumulative solute zone profile at a specified time or distance. The approaches range in complexity from the discrete plate or 'tanks-in-series' model [6–9] to the solution of detailed mass-balance equations [10–16]. A complete and rigorous model of this type requires the formulation of mathematical equations (with associated boundary conditions) which incorporate all physical and chemical processes that contribute to solute zone migration and dispersion within the separation system. These differential equations generally cannot be solved analytically in closed form and, thus, are commonly solved by numerical methods after simplifying assumptions are invoked. For example, in the equilibrium–dispersive model of mass transport [1–4], the system is considered to be in equilibrium and the dispersion from all sources is combined into a single and constant 'apparent dispersion coefficient'. In the kinetic models that allow for departure from equilibrium, the dispersion contributions are similarly combined with subsequent neglect of either the resistance to mass transfer (reaction–dispersive model) or the kinetics of adsorption/desorption (transport–dispersive model) [10]. As a consequence of these

* Corresponding author.

0021-9673/96/$15.00
SSDI 0021-9673(95)00784-9

simplifying assumptions, the classical models cannot provide a completely general description of transport phenomena in chromatographic systems. Moreover, because of their inherent macroscopic perspective, these models are inadequate to describe transport in systems that are heterogeneous at the microscopic and molecular levels.

Stochastic models have also been used to describe the evolution of the solute zone profile in the time and distance domains [4,17–20]. In these models, the random migration of a single molecule is utilized to develop probability distribution functions based on binomial or Poisson statistics, from which the cumulative zone profile can be determined. This approach can be extended to model heterogeneous separation systems by incorporating two or more independent contributions to the probability distribution functions [21,22]. Unfortunately, the resulting equations do not yield to analytical or numerical solution when all physical and chemical processes are considered, hence, simplifying assumptions are necessary. Therefore, as with the classical models, no comprehensive and completely general model is available to describe all separation systems.

Finally, a completely different stochastic approach has been utilized which, for distinction, will be called the molecular simulation models. These simulations follow the trajectories of individual molecules and range in complexity from one-dimensional models with finite step size [23–26] to three-dimensional models with variable step size [27–30]. In the most rigorous and comprehensive treatments, the fundamental equations of motion for diffusion, convection, and other transport processes are independently applied to each molecule. In contrast to the complex differential equations of mass balance, these equations of motion are relatively simple and require few, if any, simplifying assumptions. However, extremely powerful computers are required in order to model the migration of a statistically significant number of molecules over meaningful periods of time or distance. This limitation has become less severe with the routine availability of high-speed, high-memory computers, particularly those with parallel processors [31]. In recent years, three-dimensional molecular simulations have been applied to the study of flow injection analysis [27,28], field flow fractionation [29], and capillary zone electrophoresis [30].

The relationship between these three types of models may be best understood by extension of the conceptual analogy presented by McQuarrie [18]. The classical models of mass transport are related to classical thermodynamics in much the same manner that the stochastic models are to statistical thermodynamics or mechanics. In contrast, the molecular simulation approach is directly analogous to quantum mechanics, where the simpler models are semi-empirical and the more complex three-dimensional models tend to be ab initio methods. This analogy serves to clarify the advantages and limitations of each type of model, as well as to indicate its most appropriate range of applications. If the separation system is homogeneous and continuous in both spatial and temporal domains or, equivalently, can be satisfactorily described by a single set of average properties, all of these models must necessarily describe the same reality. In this case, the simplest classical or stochastic model that adequately addresses all transport processes in the system should be utilized. On the other hand, if the system is heterogeneous or discontinuous in either or both of the spatial and temporal domains, only the molecular simulation models are wholly appropriate.

In the present study, we describe the preliminary development of a three-dimensional molecular simulation that provides a unified treatment for gas, supercritical fluid, and liquid chromatography. The algorithms describing the transport phenomena have been implemented in a sequential manner, such that each may be independently validated by comparison with classical models. All physical and chemical parameters that are routinely used to control these transport phenomena are invoked as intrinsic and independent variables. Thus, this simulation provides a powerful and versatile means to examine and characterize the behavior of complex separation systems.

2. Description and validation of computer simulation

The three-dimensional molecular simulation program was developed in the FORTRAN 77 programming language and optimized for execution on an IBM RS/6000 Model 580 computer. As shown in the flowchart in Fig. 1, this program incorporates algorithms for the processes of diffusion, convection, and retention, which are repeated for each molecule at each time increment (t) until the total simulation time (T) is reached. The simulation may be performed in Cartesian global coordinates, which is most appropriate for separations in planar media, or alternatively in cylindrical global coordinates for separations in capillary tubes or fibers. Because of its mathematical simplicity, the latter case will be described in detail.

2.1. Simulation input

The input parameters required for the simulation may be divided into three general categories, as shown in Table 1. The system parameters describe properties of the fluid (mobile phase) and surface (stationary phase), as well as the spatial dimensions of the separation system to be simulated. The molecular parameters describe attributes of the solute molecules, and the computational parameters describe certain constraints that are required for the simulation. On the basis of these input parameters, an array is created that contains the properties and coordinates of each molecule. To initialize the simulation, the molecules are distributed randomly with a delta, rectangular, or Gaussian profile of specified variance at a specified mean distance in the global coordinate frame.

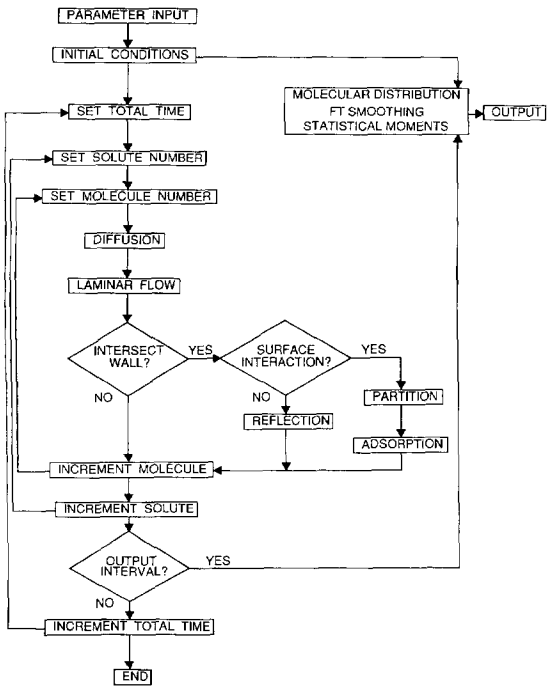

Fig. 1. Flowchart of the computer simulation program.

Table 1
List of variable simulation parameters

System parameters:	
Radius of fluid phase	R
Length of fluid phase	L
Viscosity of fluid phase	η
Mean linear velocity of fluid phase	v_0
Depth of surface phase	d_s
Pressure	P
Temperature	T_0
Molecular parameters:	
Diffusion coefficient	D_f, D_s
Distribution coefficient	K
Adsorption energy	E
Mean desorption time	τ_d
Computational parameters:	
Number of molecules	N
Molecular-frame coordinates	ρ, ϕ, θ
Global-frame coordinates:	
cylindrical	r, θ, z
Cartesian	x, y, z
Time increment	t
Total simulation time	T

2.2. Simulation output

The program allows the molecular zone profile to be examined as the distance distribution at specified simulation times or, correspondingly, as the time distribution at specified distances. The statistical moments of the molecular distribution are calculated in length units for simulations at

specified times (or in time units at specified distances). For example, the first statistical moment or mean distance (z) is determined from:

$$z = N^{-1}\sum_{i=1}^{N} z_i \quad (1)$$

the second statistical moment or variance (σ^2) is determined from:

$$\sigma^2 = N^{-1}\sum_{i=1}^{N}(z_i - z)^2 \quad (2)$$

and the higher-order statistical moments are determined in a similar manner [32], where z_i is the axial coordinate of an individual molecule and N is the total number of molecules. These statistical moments, as well as the chromatographic figures of merit derived therefrom, are stored in a standard data file at each specified time (or distance).

In addition to the numerical output parameters, the molecular population is summed in discrete length (or time) segments and then smoothed by Fourier transform methods [33] to provide a continuous zone profile for graphical display. An example of the molecular distribution and the corresponding discrete and smoothed zone profiles is illustrated in Fig. 2.

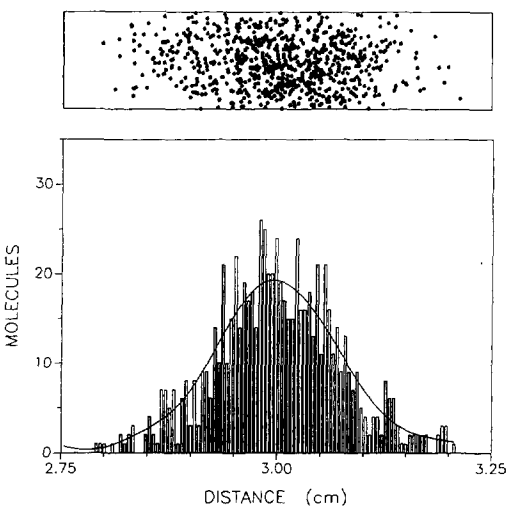

Fig. 2. Molecular distribution along the fluid–surface interface (top), together with the segmented and smoothed zone profiles (bottom).

Because the molecular distribution may be examined at any time (or distance), these output routines provide an extensive visual and numerical record of transport processes throughout the simulation.

2.3. Diffusion

Molecular diffusion is simulated by using a three-dimensional extension of the one-dimensional Einstein–Smoluchowski equation [34–36]. If each dimension is fully independent, then the radial distance ρ travelled during the time increment t is given by:

$$\rho = (6D_{f,s}t)^{1/2} \quad (3)$$

where $D_{f,s}$ represents the binary diffusion coefficient of the molecule in the fluid or surface phase, as appropriate. The direction of travel is subsequently randomized through the spherical coordinate angles (ϕ,θ). Finally, the coordinate increments in the molecular frame are used to calculate the new molecular position in the global coordinate frame.

To verify the accuracy of the diffusion algorithm, the zone distance and variance for an ensemble of 750 molecules were monitored as a function of the simulation time. These results were compared with theoretical predictions based on the Einstein equation [34]. As shown in Fig. 3, excellent agreement is observed for the range of diffusion coefficients commonly encountered in gas, supercritical fluid, and liquid chromatography (10^{-1} to 10^{-8} cm^2 s^{-1}). The average relative errors for the zone distance and variance are 0.32% and 2.96%, respectively.

2.4. Convection

Molecular convection in the fluid phase may be induced by means of a pressure gradient applied tangentially to the surface phase. Under these conditions, the radial position r of the molecule remains constant and the axial distance z travelled in time increment t is given by:

$$z = vt \quad (4)$$

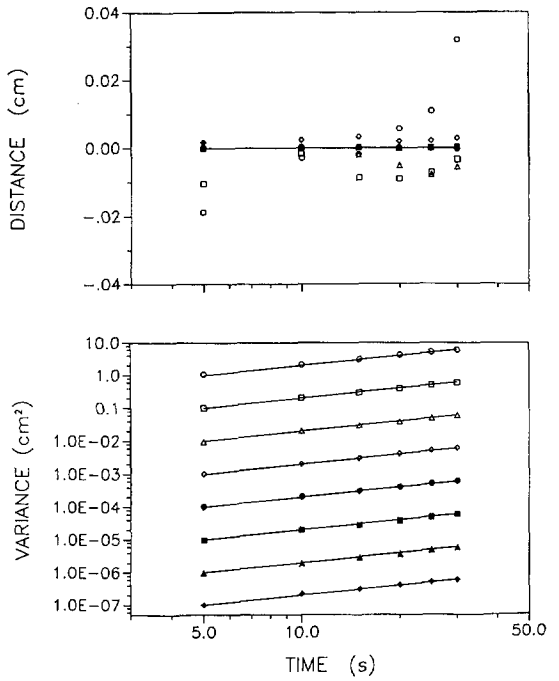

Fig. 3. Validation of the diffusion algorithms by comparison of the zone distance and variance with theoretical prediction. Simulation conditions: $N = 750$; $t = 5.0 \cdot 10^{-5}$–$1.0 \cdot 10^{-7}$ s; $R = 20.0 \cdot 10^{-4}$ cm; $D_f = 1.0 \cdot 10^{-1}$ cm^2 s^{-1} (○), $1.0 \cdot 10^{-2}$ cm^2 s^{-1} (□), $1.0 \cdot 10^{-3}$ cm^2 s^{-1} (△), $1.0 \cdot 10^{-4}$ cm^2 s^{-1} (◇), $1.0 \cdot 10^{-5}$ cm^2 s^{-1} (●), $1.0 \cdot 10^{-6}$ cm^2 s^{-1} (■), $1.0 \cdot 10^{-7}$ cm^2 s^{-1} (▲), $1.0 \cdot 10^{-8}$ cm^2 s^{-1} (◆). Theory (solid line) based on the Einstein equation [34]: $z = 0$; $\sigma^2 = 2D_t T$.

For pressure-induced flow under fully developed laminar conditions, the radial velocity profile in the cylindrical global frame is given by the Taylor–Aris equation [37,38]:

$$v = 2v_0\left[1 - \left(\frac{r}{R}\right)^2\right] \tag{5}$$

The mean velocity v_0 may be specified as an input parameter or may be calculated from the Hagen–Poiseuille equation [1–3,39]:

$$v_0 = \frac{R^2 P}{8\eta L} \tag{6}$$

where P is the applied pressure, η is the viscosity of the fluid phase, and R and L are the radius and length, respectively, of the fluid phase in the cylindrical global frame.

To verify the accuracy of the laminar convection algorithm, the zone distance and variance for an ensemble of 750 molecules were monitored as a function of the simulation time. These results were compared with theoretical predictions based on the Taylor–Aris equation [37,38] with both diffusion and resistance to mass transfer in the fluid phase. As shown in Fig. 4, excellent agreement is observed for the range of linear velocities commonly encountered in gas, supercritical fluid, and liquid chromatography (0.001 to 100.0 cm s^{-1}). The average relative errors for the zone distance and variance are 0.49% and 2.24%, respectively.

2.5. Retention

Molecular interaction is simulated as a partition process if the surface is permeable (e.g., thin

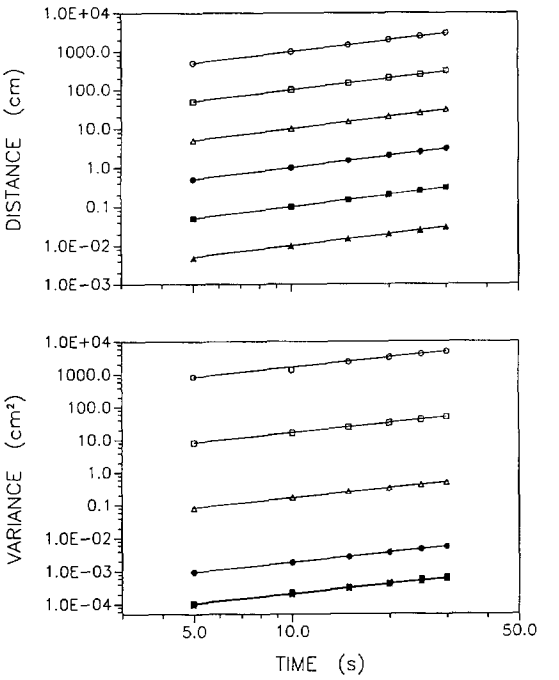

Fig. 4. Validation of the convection algorithms for pressure-induced flow under laminar conditions by comparison of the zone distance and variance with theoretical prediction. Simulation conditions: $N = 750$; $t = 5.0 \cdot 10^{-5}$ s; $R = 20.0 \cdot 10^{-4}$ cm; $D_f = 1.0 \cdot 10^{-5}$ cm^2 s^{-1}; $v_0 = 0.001$ cm s^{-1} (▲), 0.01 cm s^{-1} (■), 0.1 cm s^{-1} (●), 1.0 cm s^{-1} (△), 10.0 cm s^{-1} (□), 100.0 cm s^{-1} (○). Theory (solid line) based on the Taylor–Aris equation [37,38]: $z = v_0 T$; $\sigma^2 = 2D_t T + R^2 v_0^2 T/24D_t$.

polymer film or chemically bonded organic ligands) or as an adsorption process if the surface is solid (e.g., silica or alumina).

For the partition process, the probability of transport between the fluid and surface phases is given by:

$$P_{f-s} = K\left(\frac{D_s}{D_f}\right)^{1/2} \text{ and } P_{s-f} = 1 \quad (7a)$$

or, alternatively:

$$P_{f-s} = 1 \text{ and } P_{s-f} = K^{-1}\left(\frac{D_f}{D_s}\right)^{1/2} \quad (7b)$$

as shown graphically in Fig. 5. Because the probabilities P_{f-s} and P_{s-f} must be less than or equal to unity, the appropriate expressions (Eq. (7a) or (7b)) may be selected based on knowledge of the distribution coefficient K and the diffusion coefficients in the fluid and surface phases, D_f and D_s, respectively. When a molecule in the fluid phase encounters the fluid–surface interface during the simulation, a random number ξ between zero and one is selected. If the selected number is less than or equal to the probability P_{f-s} given by Eq. (7a) or (7b), the molecule will be transferred to the surface phase. Otherwise, the molecule will remain in the fluid phase and will undergo an elastic collision at the interface. A similar routine is performed when a molecule in the surface phase encounters the interface, except that the random number ξ is compared with the probability P_{s-f} given in Eq. (7a) or (7b). Finally, when a molecule in the fluid or surface phase encounters a spatial boundary of the system, an elastic collision is performed.

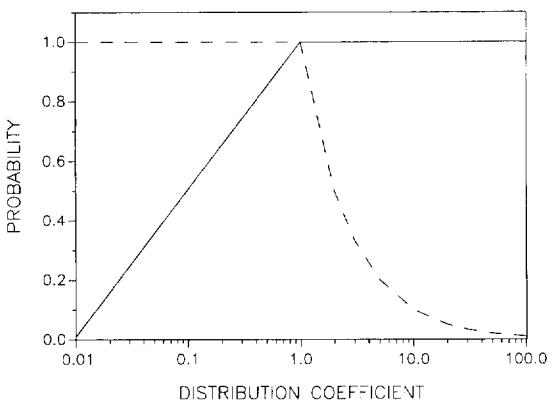

Fig. 5. Probability of transport between fluid and surface phases (P_{f-s}, solid line) and between surface and fluid phases (P_{s-f}, dashed line) as a function of the distribution coefficient for equilibrium partition mechanism.

To verify the accuracy of the retention algorithm for equilibrium partition, the ratio of molecules in the fluid and surface phases was monitored as a function of the distribution coefficient, diffusion coefficients, fluid and surface phase depths, etc. As shown in Table 2, excellent agreement is observed between the computer simulation and theoretical predictions for a wide range of experimental conditions encountered in chromatography.

To verify the accuracy of this retention algorithm in combination with the diffusion and convection algorithms, the zone distance and variance for an ensemble of 750 molecules were monitored as a function of the simulation time. These results were compared with theoretical predictions based on the extended Golay equation [13] with diffusion and resistance to mass transfer in the fluid and surface phases. As shown in Fig. 6, excellent agreement is observed for the range of distribution coefficients commonly encountered in chromatography (0.01 to 100.0). The average relative errors for the zone distance and variance are 0.55% and 4.02%, respectively.

For preliminary simulations of the adsorption process, the surface is considered as a uniform distribution of localized lattice sites, each of equal area and equal energy of interaction with the molecule. The molar adsorption energy for simple aliphatic and aromatic molecules on silica and alumina surfaces is well documented in the literature [40]. The adsorption energy E is related to the mean time for desorption τ_d in the following manner [41–43]:

$$\tau_d = \tau_0 \exp\left(\frac{E}{k_A k_B T_0}\right) \quad (8)$$

where τ_0 is the vibrational period, typically 10^{-12}–10^{-13} s, T_0 is the absolute temperature, k_B is the Boltzmann constant, and k_A is the

Table 2
Verification of the retention algorithm by comparison of the molecular distribution between the fluid and surface phases

R (cm)	d_s (cm)	K	D_f ($cm^2\ s^{-1}$)	D_s ($cm^2\ s^{-1}$)	N_s/N_f Theory[a]	N_s/N_f Simulation	Error (%)
$20.0 \cdot 10^{-4}$	$8.28 \cdot 10^{-4}$	0.1	$1.0 \cdot 10^{-5}$	$1.0 \cdot 10^{-5}$	0.10	0.10 ± 0.01	0.0
$20.0 \cdot 10^{-4}$	$8.28 \cdot 10^{-4}$	0.5	$1.0 \cdot 10^{-5}$	$1.0 \cdot 10^{-5}$	0.50	0.49 ± 0.01	−2.0
$20.0 \cdot 10^{-4}$	$8.28 \cdot 10^{-4}$	1.0	$1.0 \cdot 10^{-5}$	$1.0 \cdot 10^{-5}$	1.00	0.99 ± 0.01	−1.0
$20.0 \cdot 10^{-4}$	$8.28 \cdot 10^{-4}$	5.0	$1.0 \cdot 10^{-5}$	$1.0 \cdot 10^{-5}$	5.00	5.03 ± 0.01	0.6
$20.0 \cdot 10^{-4}$	$0.98 \cdot 10^{-4}$	1.0	$1.0 \cdot 10^{-5}$	$1.0 \cdot 10^{-6}$	0.10	0.10 ± 0.01	0.0
$20.0 \cdot 10^{-4}$	$8.28 \cdot 10^{-4}$	1.0	$1.0 \cdot 10^{-5}$	$1.0 \cdot 10^{-6}$	1.00	1.00 ± 0.01	0.0
$20.0 \cdot 10^{-4}$	$28.98 \cdot 10^{-4}$	1.0	$1.0 \cdot 10^{-5}$	$1.0 \cdot 10^{-6}$	5.00	4.97 ± 0.01	−0.6
$40.0 \cdot 10^{-4}$	$16.57 \cdot 10^{-4}$	1.0	$1.0 \cdot 10^{-5}$	$1.0 \cdot 10^{-6}$	1.00	1.01 ± 0.01	1.0
$60.0 \cdot 10^{-4}$	$24.85 \cdot 10^{-4}$	1.0	$1.0 \cdot 10^{-5}$	$1.0 \cdot 10^{-6}$	1.00	0.98 ± 0.01	−2.0
$80.0 \cdot 10^{-4}$	$33.14 \cdot 10^{-4}$	1.0	$1.0 \cdot 10^{-5}$	$1.0 \cdot 10^{-6}$	1.00	0.96 ± 0.01	−4.0

[a] Calculated as $K(V_s/V_f)$, where $V_f = \pi R^2 L$ and $V_s = \pi(d_s^2 + 2Rd_s)L$.

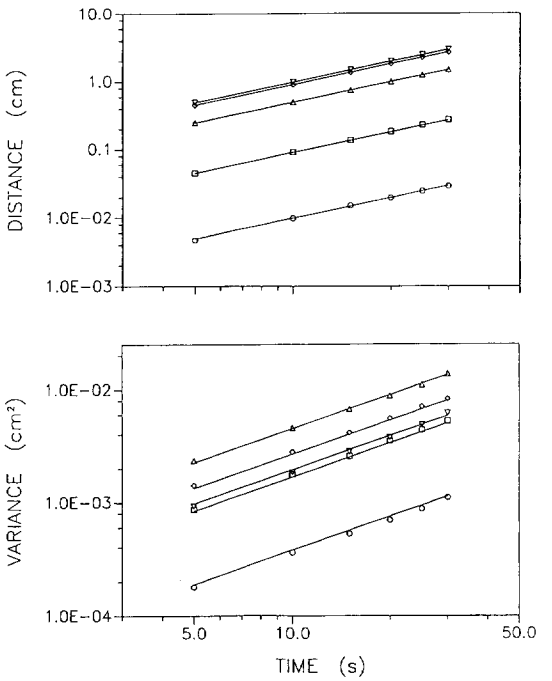

Fig. 6. Validation of the surface interaction algorithms for equilibrium partition by comparison of the zone distance and variance with theoretical prediction. Simulation conditions: $N = 750$; $t = 5.0 \cdot 10^{-5}$ s; $R = 20.0 \cdot 10^{-4}$ cm; $d_s = 8.28 \cdot 10^{-4}$ cm; $D_f = 1.0 \cdot 10^{-5}$ $cm^2\ s^{-1}$; $D_s = 1.0 \cdot 10^{-5}$ $cm^2\ s^{-1}$; $v_0 = 0.1$ $cm\ s^{-1}$; $K = 0.01$ (▽), 0.1 (◇), 1.0 (△), 10.0 (□), 100.0 (○). Theory (solid line) based on the extended Golay equation [13]: $z = v_0 T/(1+k)$; $\sigma^2 = (2D_f T) + (2D_s kT) + (1 + 6k + 11k^2)\, R^2 v_0^2\, T/24\,(1+k)^2\, D_f + 2kd_s^2 v_0^2 T/3\,(1+k)^2 D_s$, where $k = K[(d_s^2 + 2Rd_s)/R^2]$.

Avogadro constant. If a molecule encounters the surface, the probability for adsorption P_{f-s} is equal to unity if the site is vacant and zero if it is occupied [44,45]. The probability for desorption P_{s-f} is determined in one of the following ways: (1) a simple random-walk approach in which the probability is zero when the incremental time is less than the mean desorption time and is unity thereafter; and (2) a Poisson distribution for the probability in which the mean value and standard deviation are defined by the desorption time [30]. These algorithms may be readily extended to heterogeneous surfaces that consist of two or more types of lattice sites having different area and different energy of interaction with the molecule [46,47].

3. Applications of computer simulation

Based on the validation studies described above, the computer simulation accurately models the diffusion, convection, and retention processes that occur during chromatographic separations. Consequently, it may now be applied with confidence to examine and characterize the separation mechanism in greater detail. Because this simulation monitors the migration of individual molecules, it provides the opportunity to perform simulated experiments and to make observations that may not be possible in a

real chromatographic system. For example, kinetic rate constants for the separation process may be directly determined and their dependence upon the simulation variables may be readily established. In addition, retention and dispersion arising in regions of discrete spatial and temporal transition may be examined. The preliminary studies described herein will focus on characterization of the partition mechanism under conditions representative of liquid chromatography, with later studies to be focused on the adsorption mechanism [48]. Once these retention mechanisms have been individually examined and characterized, the simulation can then be applied to elucidate the composite partition–adsorption mechanism.

3.1. Determination of kinetic rate constants

In the partition process, the solute X is distributed between the fluid and surface phases by a reversible mechanism:

$$X_f \underset{k_{s-f}}{\overset{k_{f-s}}{\rightleftharpoons}} X_s \tag{9}$$

where k_{f-s} and k_{s-f} are the first-order rate constants. When the system is in equilibrium, the ratio of the number of solute molecules in the fluid (N_f) and surface (N_s) phases defines the distribution coefficient:

$$\frac{K V_s}{V_f} = \frac{N_s}{N_f} = \frac{k_{f-s}}{k_{s-f}} \tag{10}$$

which is adjusted for the relative volumes of the fluid (V_f) and surface (V_s) phases. Prior to equilibrium, however, the distribution of solute molecules can be described by a kinetic model of reversible reactions [43,49]. Under these conditions, the net rate of change in the number of molecules in the fluid phase is:

$$\frac{d(N_f)}{dT} = -k_{f-s} N_f + k_{s-f} N_s \tag{11}$$

If all molecules initially reside in the fluid phase, the solution of Eq. (11) is given by:

$$\frac{(N_f)_T}{(N_f)_0} = \frac{k_{s-f} + k_{f-s} \exp[-T(k_{f-s} + k_{s-f})]}{k_{f-s} + k_{s-f}} \tag{12}$$

where $(N_f)_0$ and $(N_f)_T$ are the number of molecules remaining in the fluid phase at time 0 and T, respectively. Hence, the distribution of molecules between the fluid and surface phases can be predicted at any time by using Eq. (12) if the rate constants are known. Conversely, the rate constants can be predicted if the distribution is known as a function of time. Whereas neither of these cases is amenable to direct experimental measurement in a chromatographic system, both may be readily examined by means of the three-dimensional molecular simulation.

An example of the latter case is illustrated in Fig. 7, where the relative number of molecules in the fluid phase is shown as a function of the simulation time. From nonlinear regression analysis of the simulation data in the center curve ($K = 2.0$, $V_f/V_s = 2.0$), the rate constants k_{f-s} and k_{s-f} are determined to be 8.37 and 8.56 s^{-1}, respectively. Although the probability of molecular transfer from the fluid to the surface phase ($P_{f-s} = 0.63$) is less than that from surface to fluid ($P_{s-f} = 1.00$) according to Eq. (7a), the rate constants are equal because of the commensurately larger volume of the fluid phase. The ratio of these rate constants ($k_{f-s}/k_{s-f} = 0.98$) is in accord with the ratio of the number of molecules in the surface and fluid phase after equilibrium has

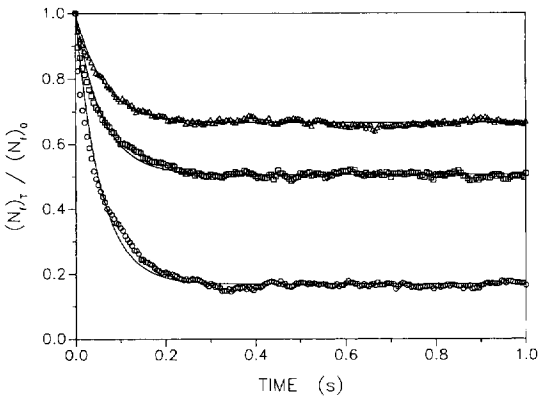

Fig. 7. Determination of the rate of solute equilibration from the relative number of molecules in the fluid phase as a function of simulation time. Simulation conditions: $N = 1000$; $t = 5.0 \cdot 10^{-5}$ s; $R = 20.0 \cdot 10^{-4}$ cm; $d_s = 4.49 \cdot 10^{-4}$ cm; $D_f = 1.0 \cdot 10^{-5}$ cm^2 s^{-1}; $D_s = 1.0 \cdot 10^{-6}$ cm^2 s^{-1}; $v_0 = 0.0$ cm s^{-1}; $K = 1.0$ (△), 2.0 (□), 10.0 (○). Solid lines show nonlinear regression analysis according to Eq. (12).

been reached ($N_s/N_f = 0.99$). Moreover, both the kinetic and equilibrium descriptions of the molecular distribution show excellent agreement with the theoretically expected value ($K\,(V_s/V_f) = 1.00$) from Eq. (10). Upon substitution of these rate constants into Eq. (11), the principle of detailed balance reveals that each molecule is transferred between the fluid and surface phases an average of 4.2 times per second at equilibrium.

The results obtained from other simulations with varying distribution coefficient, but all other conditions remaining constant, are summarized in Fig. 7 and Table 3. For a rapidly reversible partition mechanism, these rate constants represent diffusion-limited conditions; i.e., the rate constant k_{f-s} is controlled by diffusional mass transport in the fluid phase and the rate constant k_{s-f} by that in the surface phase. Under these conditions, Fig. 7 illustrates that the number of molecules in the fluid phase reaches $1-(1/e)$ of its final value after approximately 0.06 s and that equilibration is virtually complete after 0.30 s.

From these types of simulations, a greatly improved understanding is derived of the kinetic processes involved in chromatographic separations. This understanding is essential if the dispersion processes inherent in chromatographic systems are to be minimized. For example, these rate constants give a direct indication of the relative magnitude and importance of the fluid- and surface-phase mass transfer contributions to dispersion. The simulation permits facile examination of the effect of variables such as radius of the fluid phase, depth of the surface phase, distribution coefficient, diffusion coefficients, etc., on these sources of dispersion. The rate constants are also necessary to evaluate the effect of a discrete spatial or temporal transition on the solute zone profile, as discussed in the following sections.

3.2. Nonequilibrium during injection and elution processes

After any rapid change in the physical or chemical environment, some time is necessary before equilibrium can be reestablished. In chromatographic systems, such nonequilibrium conditions exist to some extent continually as the solute zone travels along the column [25]. However, a further departure from equilibrium occurs specifically upon injection to and elution from the column. During these processes, the solute zone encounters a spatially distinct region in which its retention is abruptly and permanently altered. This transition may be beneficial for chromatographic resolution and detection sensitivity if the resultant solute zone is compressed, or detrimental if the zone is expanded.

In previous studies, a classical steady-state model was developed to describe nonequilibrium during the injection [50] and elution [51] processes:

$$\sigma_f^2 = \left(\frac{R_i^2\,[1 + K_i\,(V_s/V_f)]}{R_f^2\,[1 + K_f\,(V_s/V_f)]} \right)^2 \sigma_i^2 \qquad (13)$$

where σ_i^2 and σ_f^2 are the initial and final variance of the solute zone during the transition between regions with radius R_i and R_f, and solute distribution coefficient K_i and K_f, respectively. This

Table 3
Kinetic rate constants k_{f-s} and k_{s-f} determined by numerical regression analysis of the simulation data shown in Fig. 7 to Eq. (12) (these rate constants represent conditions of diffusion-limited mass transport)

K	V_f/V_s	k_{f-s} (s^{-1})	k_{s-f} (s^{-1})	k_{f-s}/k_{s-f}	N_s/N_f
0.5	2.0	2.87 ± 0.06	11.46 ± 0.24	0.25	0.25
1.0	2.0	5.25 ± 0.08	10.46 ± 0.17	0.50	0.50
2.0	2.0	8.37 ± 0.14	8.56 ± 0.15	0.98	0.99
5.0	2.0	13.29 ± 0.20	5.34 ± 0.10	2.49	2.56
10.0	2.0	15.38 ± 0.24	3.13 ± 0.07	4.92	5.04

steady-state model assumes that the entire solute zone is influenced simultaneously rather than progressively by the spatial transition and that no other sources of dispersion occur in this region. These assumptions are clearly an over-simplification, since dispersion from mass transport processes in the cylindrical column must occur as well. If the column dispersion processes are fully independent, then the variance may be calculated by using the classical equations developed by Taylor and Aris [37,38] for a nonretained solute or by Golay [13] for a retained solute. However, because both column dispersion and nonequilibrium dispersion processes are a function of the distribution coefficient, these contributions must be considered concurrently. The three-dimensional molecular simulation permits a more rigorous and detailed examination of these injection and elution effects.

In order to accomplish this goal, it is necessary to modify the simulation program to incorporate discrete spatial transitions (i.e., discontinuous functions of a simulation variable, such as distribution coefficient, that arise at a specified distance). In this program, time has been chosen as the independent and discrete variable, whereas distance is the dependent and continuous variable. Therefore at each time increment, the position of each molecule must be determined before invoking a distance-dependent function for the distribution coefficient or other variable. This approach has been successfully employed for some preliminary simulations of the injection and elution processes. The chromatographic conditions chosen for these simulations are similar to those described in Fig. 7 and Table 3, for which the diffusion-limited rate constants have already been determined under static conditions. For a relatively slow linear velocity of 0.1 cm s^{-1}, the solute zone will travel only 0.03 cm within the time required for complete equilibration (vide supra). Thus, these conditions ensure that steady-state behavior will be maintained along the chromatographic column.

Upon injection, the solute zones encounter an abrupt spatial transition from the nonretained state ($K_i = 0.0$) to the retained state ($K_f = 1.0$, 2.0, 10.0). The solute zone profiles, together with their corresponding variances, are evaluated at five simulation times during this transition (Fig. 8). The initial profile is evaluated in the nonretentive region and, hence, is identical for all solute zones. The second through fourth profiles are assessed during the transition, whereas the final profile is evaluated when the solute zone is completely within the retentive region. Because the average linear velocity of molecules is reduced after the transition, the resultant solute zone is compressed by the nonequilibrium process. The extent of compression clearly increases with the distribution coefficient, as indicated by the decrease in variance and increase in amplitude between the initial and final zone profiles.

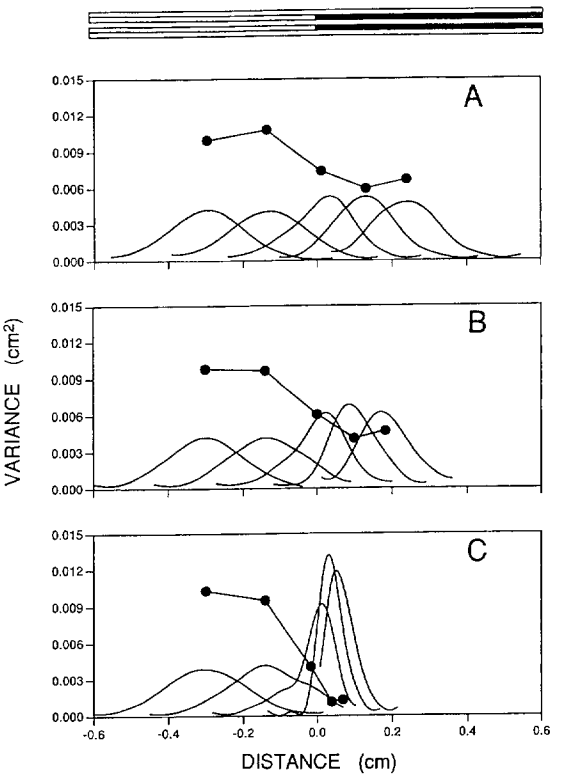

Fig. 8. Solute zone profiles, together with their corresponding variances (●), during the injection process. Column inlet is at 0.0 cm, as shown in schematic diagram at top. Simulation conditions: $N = 500$; $t = 5.0 \cdot 10^{-4}$ s; $R = 20.0 \cdot 10^{-4}$ cm; $d_s = 4.49 \cdot 10^{-4}$ cm; $D_f = 1.0 \cdot 10^{-5}$ cm^2 s^{-1}; $D_s = 1.0 \cdot 10^{-6}$ cm^2 s^{-1}; $v_0 = 0.1$ cm s^{-1}; $K_i \rightarrow K_f = 0.0 \rightarrow 1.0$ (A), $0.0 \rightarrow 2.0$ (B), $0.0 \rightarrow 10.0$ (C).

The effect of column dispersion processes, which are also dependent upon distribution coefficient but serve to increase the variance and decrease the amplitude, is most evident between the fourth and fifth zone profiles. The results of these simulations are summarized and compared with the classical models in Table 4. It is clear that the simple steady-state model in Eq. (13) exaggerates the compression effect of injection nonequilibrium and significantly underestimates the final variance. When column dispersion processes are included, the Taylor–Aris equation [37,38] for a nonretained solute underestimates the variance whereas the extended Golay equation [13] for a retained solute overestimates the variance.

The complementary elution effect is shown in Fig. 9, where the solute zones encounter an abrupt spatial transition from the retained state (K_i = 1.0, 2.0, 10.0) to the nonretained state (K_f = 0.0). The initial profile is evaluated in the retentive region, the second through fourth profiles during the transition, and the final profile in the nonretentive region. Because the average linear velocity of molecules increases after the transition, the resultant solute zone is expanded by the nonequilibrium process. The extent of expansion increases dramatically with the distribution coefficient, as revealed by the change in variance and amplitude between the initial and final profiles. The results of these simulations are summarized and compared with the classical models in Table 4. It is evident that the simple steady-state model in Eq. (13) underestimates the expansion effect of elution nonequilibrium, and neither the Taylor–Aris [37,38] nor the Golay equation [13] adequately addresses the contributions from column processes. Because this source of dispersion is an important contribution to the general elution problem in chromatography [39], further investigation is clearly warranted.

Table 4
Initial and final zone variance arising from nonequilibrium processes during injection (Fig. 8), elution (Fig. 9), and stepwise gradients (Figs. 10 and 11)

K_i	K_f	V_i/V_s	Simulation model				Classical models		
			z_i (cm)	z_f (cm)	σ_i^2 (cm^2)	σ_f^2 (cm^2)	σ_f^2 (cm^2)[a]	σ_f^2 (cm^2)[b]	σ_f^2 (cm^2)[c]
0.0	1.0	2.0	−0.30	0.24	$9.93 \cdot 10^{-3}$	$6.64 \cdot 10^{-3}$	$4.41 \cdot 10^{-3}$	$5.42 \cdot 10^{-3}$	$7.12 \cdot 10^{-3}$
0.0	2.0	2.0	−0.30	0.18	$9.76 \cdot 10^{-3}$	$4.66 \cdot 10^{-3}$	$2.44 \cdot 10^{-3}$	$3.34 \cdot 10^{-3}$	$5.16 \cdot 10^{-3}$
0.0	10.0	2.0	−0.30	0.07	$1.03 \cdot 10^{-2}$	$1.31 \cdot 10^{-3}$	$2.86 \cdot 10^{-4}$	$9.77 \cdot 10^{-4}$	$2.08 \cdot 10^{-3}$
1.0	0.0	2.0	−0.30	0.47	$9.84 \cdot 10^{-3}$	$2.88 \cdot 10^{-2}$	$2.21 \cdot 10^{-2}$	$2.36 \cdot 10^{-2}$	$2.57 \cdot 10^{-2}$
2.0	0.0	2.0	−0.30	0.61	$9.61 \cdot 10^{-3}$	$5.58 \cdot 10^{-2}$	$3.84 \cdot 10^{-2}$	$4.01 \cdot 10^{-2}$	$4.32 \cdot 10^{-2}$
10.0	0.0	2.0	−0.30	1.83	$9.69 \cdot 10^{-3}$	$5.04 \cdot 10^{-1}$	$3.49 \cdot 10^{-1}$	$3.53 \cdot 10^{-1}$	$3.58 \cdot 10^{-1}$
10.0	1.0	2.0	0.00	0.32	$9.72 \cdot 10^{-3}$	$3.91 \cdot 10^{-3}$	$1.56 \cdot 10^{-3}$	$2.14 \cdot 10^{-3}$	–
10.0	2.0	2.0	0.00	0.25	$9.53 \cdot 10^{-3}$	$6.04 \cdot 10^{-3}$	$3.43 \cdot 10^{-3}$	$3.90 \cdot 10^{-3}$	–
2.0	1.0	2.0	0.00	0.73	$1.01 \cdot 10^{-2}$	$9.95 \cdot 10^{-3}$	$4.49 \cdot 10^{-3}$	$5.85 \cdot 10^{-3}$	–
1.0	10.0	2.0	0.00	0.78	$9.41 \cdot 10^{-3}$	$9.18 \cdot 10^{-2}$	$5.88 \cdot 10^{-2}$	$6.03 \cdot 10^{-2}$	–
2.0	10.0	2.0	0.00	0.43	$1.01 \cdot 10^{-2}$	$3.99 \cdot 10^{-2}$	$2.81 \cdot 10^{-2}$	$2.88 \cdot 10^{-2}$	–
1.0	2.0	2.0	0.00	1.08	$9.26 \cdot 10^{-3}$	$3.78 \cdot 10^{-2}$	$2.08 \cdot 10^{-2}$	$2.29 \cdot 10^{-2}$	–

[a] Calculated by using Eq. (13) or (14) for nonequilibrium dispersion.
[b] Calculated by using Eq. (13) or (14) for nonequilibrium dispersion and the Taylor–Aris equation [37,38] for column dispersion of a nonretained solute.
[c] Calculated by using Eq. (13) or (14) for nonequilibrium dispersion and the extended Golay equation [13] for column dispersion of a retained solute.

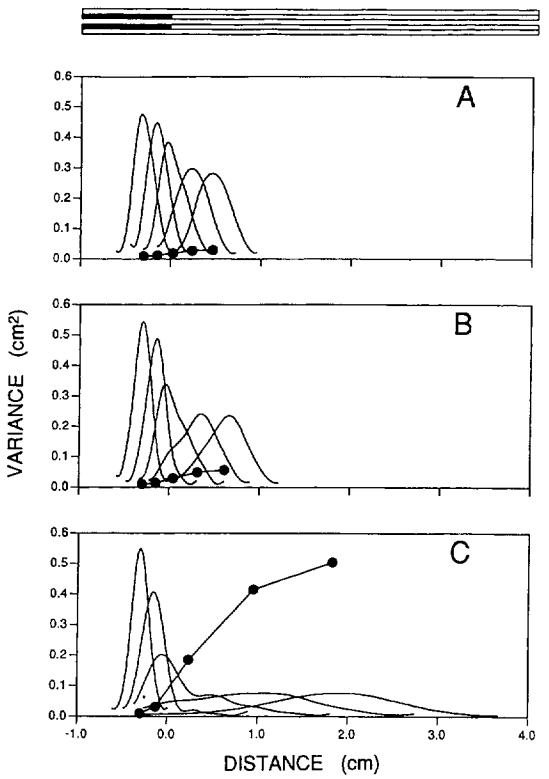

Fig. 9. Solute zone profiles, together with their corresponding variances (●), during the elution process. Column outlet is at 0.0 cm, as shown in schematic diagram at top. Simulation conditions: $N = 500$; $t = 5.0 \cdot 10^{-4}$ s; $R = 20.0 \cdot 10^{-4}$ cm; $d_s = 4.49 \cdot 10^{-4}$ cm; $D_f = 1.0 \cdot 10^{-5}$ cm^2 s^{-1}; $D_s = 1.0 \cdot 10^{-6}$ cm^2 s^{-1}; $v_0 = 0.1$ cm s^{-1}; $K_i \rightarrow K_f = 1.0 \rightarrow 0.0$ (A), $2.0 \rightarrow 0.0$ (B), $10.0 \rightarrow 0.0$ (C).

3.3. Nonequilibrium during stepwise and linear gradients

It is also desirable to examine dispersion processes during more complex transitions, such as a stepwise or linear gradient in velocity, temperature, or solvent composition. The classical steady-state model yields the following expression to describe nonequilibrium dispersion under such conditions [52,53]:

$$\sigma_f^2 = \left(\frac{K_f [1 + K_i (V_s/V_f)]}{K_i [1 + K_f (V_s/V_f)]} \right)^2 \sigma_i^2 \qquad (14)$$

for a cylindrical column with constant radius. As in the previous cases, this model assumes that the entire solute zone is influenced simultaneously by the transition and that no other sources of dispersion occur. The column dispersion processes for a nonretained solute may be calculated by using the Taylor–Aris equation [37,38]. However, it is not possible to estimate the additional dispersion for a retained solute by means of the Golay equation [13] because the spatial position of the transition is not constant or known.

In order to characterize these stepwise and linear gradients by means of the three-dimensional molecular simulation, it is necessary to incorporate two additional types of transitions: temporal transitions (i.e., discontinuous or continuous functions of a simulation variable, such as distribution coefficient, that arise at a specified time) and nonstationary spatiotemporal transitions (i.e., discontinuous or continuous functions of the variable that are not fixed in either distance or time, but migrate at a linear velocity different from that of the solute zone). Because time has been chosen as the independent variable for this simulation, temporal transitions may be achieved directly by invoking a time-dependent function for the variable. In contrast, nonstationary transitions present a more complicated and time-consuming computational problem because, at each time increment, the position of each molecule as well as that of the transition itself must be determined before invoking a distance-dependent function for the variable. Some preliminary results are described below in which discontinuous functions of the distribution coefficient are considered as nonstationary transitions. These simulations are representative of practical conditions such as injection of a solute in a solvent other than the fluid phase, as well as stepwise gradients in composition of the fluid phase.

The simulation conditions are similar to those described in Fig. 7 and Table 3, for which the diffusion-limited rate constants have already been determined. As noted previously, steady-state behavior will be maintained under these conditions at a linear velocity of 0.1 cm s^{-1}. The first sequence of simulations, shown in Fig. 10, is representative of a stepwise increase in solvent strength. During this transition, the distribution

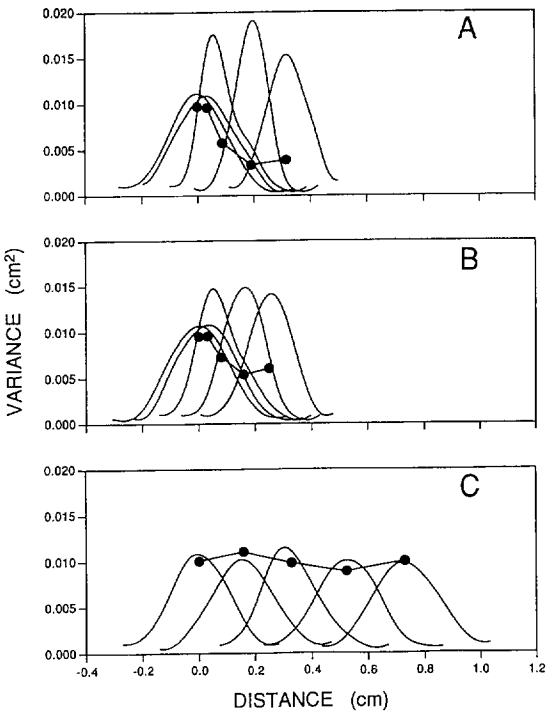

Fig. 10. Solute zone profiles, together with their corresponding variances (●), during a stepwise increase in solvent strength. Simulation conditions: $N = 500$; $t = 5.0 \cdot 10^{-4}$ s; $R = 20.0 \cdot 10^{-4}$ cm; $d_s = 4.49 \cdot 10^{-4}$ cm; $D_f = 1.0 \cdot 10^{-5}$ cm^2 s^{-1}; $D_s = 1.0 \cdot 10^{-6}$ cm^2 s^{-1}; $v_0 = 0.1$ cm s^{-1}; $K_i \rightarrow K_f = 10.0 \rightarrow 1.0$ (A), $10.0 \rightarrow 2.0$ (B), $2.0 \rightarrow 1.0$ (C).

coefficient of the solute decreases ($K_i \rightarrow K_f = 10.0 \rightarrow 1.0$, $10.0 \rightarrow 2.0$, $2.0 \rightarrow 1.0$), whereas that of the solvent remains constant (0.0). The solute zone profiles, together with their corresponding variances, are evaluated periodically throughout the transition. In the initial profile, the transition between solvent zones is located at the rear boundary of the solute zone. Because the solvent zone migrates at a higher linear velocity, it gradually surpasses the solute zone so that, in the final profile, the transition is located at the front boundary of the solute zone. Thus, in contrast to discrete temporal transitions where the entire solute zone is influenced simultaneously, and discrete spatial transitions where the solute zone is influenced progressively from the front boundary, in most practical applications of nonstationary transitions, the solute zone is influenced progressively from the rear boundary. The average linear velocity of molecules increases after the transition to higher solvent strength, hence the resultant solute zone is compressed by the nonequilibrium process. Several important conclusions are evident in this sequence of simulations. First, the greater the ratio of distribution coefficients in the initial and final solvents, the greater the extent of solute zone compression. If the distribution coefficient changes too significantly, however, the solute zone profile may exhibit severe distortion and asymmetry during the transition (Fig. 10A and 10B, second and third profiles). Finally, the greater the magnitude of the initial and final distribution coefficients, the more rapidly the solute zone is surpassed by the solvent zone. The results of these simulations are summarized and compared with the classical models in Table 4.

The complementary case, shown in Fig. 11, is representative of a stepwise decrease in solvent

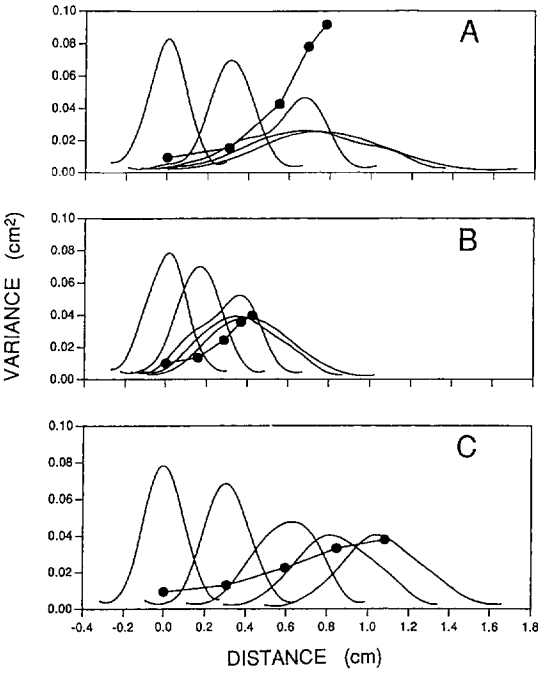

Fig. 11. Solute zone profiles, together with their corresponding variances (●), during a stepwise decrease in solvent strength. Simulation conditions: $N = 500$; $t = 5.0 \cdot 10^{-4}$ s; $R = 20.0 \cdot 10^{-4}$ cm; $d_s = 4.49 \cdot 10^{-4}$ $D_f = 1.0 \cdot 10^{-5}$ cm^2 s^{-1}; $D_s = 1.0 \cdot 10^{-6}$ cm^2 s^{-1}; $v_0 = 0.1$ cm s^{-1}; $K_i \rightarrow K_f = 1.0 \rightarrow 10.0$ (A), $2.0 \rightarrow 10.0$ (B), $1.0 \rightarrow 2.0$ (C).

strength. During this transition, the distribution coefficient of the solute increases ($K_i \rightarrow K_f$ = 1.0 → 10.0, 2.0 → 10.0, 1.0 → 2.0), whereas that of the solvent remains constant (0.0). Because the average linear velocity of molecules decreases after the transition, the resultant solute zone is expanded by the nonequilibrium process. The smaller the ratio of distribution coefficients in the initial and final solvents, the greater the extent of solute zone expansion. Again, if the distribution coefficient changes too significantly, the solute zone profile may exhibit severe distortion and asymmetry during the transition (Fig. 11A and 11B, third and fourth profiles). The results of these simulations are summarized and compared with the classical models in Table 4.

These simulations provide additional insight into the injection process when a solvent other than the fluid phase is employed. If the solute is injected in a solvent that is weaker than the fluid phase ($K_i > K_f$), the solute zone is compressed to a greater extent during the spatial transition from the nonretentive to retentive regions at the column inlet. Then, as the injection solvent surpasses the solute zone and is replaced by the fluid phase, the zone is further compressed. The opposite effect is observed when the solute is injected in a solvent that is stronger than the fluid phase ($K_i < K_f$). During the spatial transition, the solute zone is compressed to a lesser extent; then, as the injection solvent is replaced by the fluid phase, the solute zone is further expanded. Thus, these two independent transition processes act in a cooperative manner to decrease or increase the solute zone variance during the injection process.

4. Conclusions

The three-dimensional molecular simulation program incorporates the processes of diffusion, convection, and retention by a partition or adsorption mechanism. The individual algorithms have been validated under a wide variety of representative conditions for gas, supercritical fluid, and liquid chromatography. Because of the modular nature of this program, the algorithms may be simply and rapidly modified to allow additional mass transport processes to be examined.

Because this simulation program monitors the migration of individual molecules, it provides the opportunity to perform hypothetical experiments and to make observations that may not be possible in a real chromatographic system. For example, the kinetic rate constants may be directly determined and their dependence upon variables such as the distribution coefficient, column radius, and diffusion coefficients may be readily established. In addition, retention and dispersion processes may be examined in regions of discrete spatial transition (e.g., injection and elution) as well as discrete or continuous temporal transitions (e.g., velocity, temperature, or solvent composition gradient).

One of the most significant features of the simulation program is that molecular migration is monitored in three-dimensional space. As a consequence of this spatial resolution, mass transport processes can be easily studied on surfaces with physical and chemical heterogeneity at the molecular level. In addition, mono- or multilayer systems as well as systems with domains of microscopic or macroscopic architecture can be readily accommodated. Thus, this simulation provides a powerful means to examine and characterize the kinetic and equilibrium behavior of complex separation systems.

Acknowledgements

The authors gratefully acknowledge Dr. Jon H. Wahl (Battelle Pacific Northwest Laboratories) for preliminary development of the computer program, as well as Professor Christie G. Enke (University of New Mexico) and Dr. Mark R. Schure (Rohm and Haas Company) for stimulating discussions. This research was supported by the U.S. Department of Energy, Office of Basic Energy Sciences, Division of Chemical Sciences, under contract number DE-FG02-89ER14056.

References

[1] R.B. Bird, W.E. Stewart and E.N. Lightfoot, Transport Phenomena, Wiley, New York, NY, 1960.

[2] T.K. Sherwood, R.L. Pigford and C.R. Wilke, Mass Transfer, McGraw-Hill, New York, NY, 1975.
[3] A.L. Hines and R.N. Maddox, Mass Transfer: Fundamentals and Applications, Prentice-Hall, Englewood Cliffs, NJ, 1985.
[4] S. Golshan-Shirazi and G. Guiochon, in F. Dondi and G. Guiochon (Editors), Theoretical Advancement in Chromatography and Related Separation Techniques, Kluwer, Amsterdam, 1992, pp. 61–92.
[5] S. Golshan-Shirazi and G. Guiochon, J. Chromatogr., 603 (1992) 1.
[6] L.C. Craig, J. Biol. Chem., 155 (1944) 519.
[7] A.J.P. Martin and R.L.M. Synge, Biochem. J., 35 (1941) 1358.
[8] A. Klinkenberg and F. Sjenitzer, Chem. Eng. Sci., 5 (1956) 258.
[9] A.S. Said, AIChE J., 2 (1956) 477.
[10] L. Lapidus and N.L. Amundson, J. Phys. Chem., 56 (1952) 984.
[11] J.J. van Deemter, F.J. Zuiderweg and A. Klinkenberg, Chem. Eng. Sci., 5 (1956) 271.
[12] E. Glueckauf, Trans. Faraday Soc., 51 (1955) 1540.
[13] M.J.E. Golay, in D.H. Desty (Editor), Gas Chromatography 1958, Academic Press, New York, NY, p. 36.
[14] E. Kucera, J. Chromatogr., 19 (1965) 237.
[15] C. Horvath and H.J. Lin, J. Chromatogr., 149 (1978) 43.
[16] A. Rasmuson, AIChE J., 27 (1981) 1032.
[17] J.C. Giddings and H. Eyring, J. Phys. Chem., 59 (1955) 416.
[18] D.A. McQuarrie, J. Chem. Phys., 38 (1963) 437.
[19] F. Dondi and M. Remelli, J. Phys. Chem., 90 (1986) 1885.
[20] C.P. Woodbury, J. Chromatogr. Sci., 32 (1994) 339.
[21] J.C. Giddings, J. Chem. Phys., 26 (1957) 169.
[22] J.C. Giddings, J. Chem. Phys., 31 (1959) 1462.
[23] J.C. Giddings, J. Chem. Educ., 35 (1958) 588.
[24] W.L. Jones, Anal. Chem., 33 (1961) 829.
[25] J.C. Giddings, Dynamics of Chromatography, Marcel Dekker, New York, NY, 1965.
[26] S.G. Weber, Anal. Chem., 56 (1984) 2104.
[27] D. Betteridge, C.Z. Marczewski and A.P. Wade, Anal. Chim. Acta, 165 (1984) 227.
[28] P.D. Wentzell, M.R. Bowridge, E.L. Taylor and C. MacDonald, Anal. Chim. Acta, 278 (1993) 293.
[29] M.R. Schure, Anal. Chem., 60 (1988) 1109.
[30] M.R. Schure and A.M. Lenhoff, Anal. Chem., 65 (1993) 3024.
[31] M.P. Allen and D.J. Tildesley, Computer Simulation of Liquids, Oxford University Press, Oxford, 1989.
[32] E. Grushka, M.N. Myers, P.D. Schettler and J.C. Giddings, Anal. Chem., 41 (1969) 889.
[33] W.H. Press, B.P. Flannery, S.A. Teukolsky and W.T. Vetterling, Numerical Recipes: The Art of Scientific computing, Cambridge University Press, Cambridge, 1989.
[34] A. Einstein, Ann. Phys., 17 (1905) 549.
[35] R.C. Reid, J.M. Prausnitz and T.K. Sherwood, The Properties of Gases and Liquids, McGraw-Hill, New York, NY, 1977.
[36] W. Feller, Probability Theory and its Application, Wiley, New York, NY, 1950, Ch. 14.
[37] G. Taylor, Proc. R. Soc. (London), A219 (1953) 186.
[38] R. Aris, Proc. R. Soc. (London), A235 (1956) 67.
[39] B.L. Karger, L.R. Snyder and C. Horvath, An Introduction to Separation Science, Wiley, New York, NY, 1973.
[40] L.R. Snyder, J. Chromatogr., 23 (1966) 388.
[41] D.M. Young and A.D. Crowell, Physical Adsorption of Gases, Butterworths, London, 1962.
[42] A.W. Adamson, Physical Chemistry of Surfaces, Wiley, New York, NY, 1976.
[43] J.I. Steinfeld, J.S. Francisco and W.L. Hase, Chemical Kinetics and Dynamics, Prentice Hall, Englewood Cliffs, NJ, 1989.
[44] J. Feder, J. Theor. Biol., 87 (1980) 237.
[45] J.D. Sherwood, J. Phys. A, Math. Gen., 23 (1990) 2827.
[46] A. Patrykiejew, Thin Solid Films, 139 (1986) 209.
[47] A. Patrykiejew, Thin Solid Films, 208 (1992) 189.
[48] P. Wu and V.L. McGuffin, manuscript in preparation.
[49] S.W. Benson, Foundations of Chemical Kinetics, McGraw-Hill, New York, NY, 1960.
[50] C.E. Evans and V.L. McGuffin, Anal. Chem., 63 (1991) 1393.
[51] C.E. Evans and V.L. McGuffin, J. Liq. Chromatogr., 11 (1988) 1907.
[52] L.R. Snyder and D.L. Saunders, J. Chromatogr. Sci., 7 (1969) 195.
[53] H. Poppe, J. Paanakker and M. Bronckhorst, J. Chromatogr., 204 (1981) 77.